Strain robust spin gapless semiconductors/half-metals in transition metal embedded MoSe2 monolayer

Yang, Q.; Kou, L.; Hu, X.; Wang, Y.; Lu, C.; Krasheninnikov, A.; Sun, L.;

Originally published:

June 2020

Journal of Physics: Condensed Matter 32(2020), 365305

DOI: https://doi.org/10.1088/1361-648X/ab9052

Strain robust spin gapless semiconductors/half-metals in transition metal embedded $MoSe_2$ monolayer

Qiang Yang,[1] Liangzhi Kou,[3] Xiaohui Hu,[*1,2] Yifeng Wang,[1,2] Chunhua Lu,[1,2] Arkady V. Krasheninnikov,[4,5] Litao Sun[6]

[1] College of Materials Science and Engineering, Nanjing Tech University, Nanjing 211816, China

[2] Jiangsu Collaborative Innovation Center for Advanced Inorganic Function Composites, Nanjing Tech University, Nanjing 211816, China

[3] School of Chemistry, Physics and Mechanical Engineering Faculty, Queensland University of Technology, Garden Point Campus, Brisbane, QLD 4001, Australia

[4] Institute of Ion Beam Physics and Materials Research, Helmholtz-Zentrum Dresden-Rossendorf, 01314 Dresden, Germany

[5] Department of Applied Physics, Aalto University School of Science, PO Box 11100, 00076 Aalto, Finland

[6] SEU-FEI Nano-Pico Center, Key Laboratory of MEMS of Ministry of Education, Collaborative Innovation Center for Micro/Nano Fabrication, Device and System, Southeast University, Nanjing 210096, China

Corresponding Author: xiaohui.hu@njtech.edu.cn (X Hu)

ABSTRACT

The realization of spin gapless semiconductor (SGS) and half-metal (HM) behavior in two-dimensional (2D) transition metal dichalcogenides (TMDs) is highly desirable for their applications in spintronic devices. Here, using density functional theory calculations, we demonstrate that Fe, Co, Ni substitutional impurities can not only induce magnetism in $MoSe_2$ monolayer, but also convert the semiconducting $MoSe_2$ to a SGS/HM system. We also study the effects of mechanical strain on the magnetic and electronic properties of the doped monolayer. We show that for all transition metal (TM) impurities we considered, the system exhibit the robust SGS/HM behavior regardless of biaxial strain values. Moreover, it is found that the magnetic properties of TM-$MoSe_2$ can effectively be tuned under biaxial strain by controlling the spin polarization of the 3*d* orbitals of Fe, Co, Ni atoms. Our findings offer a new route to designing the SGS/HM properties and modulating magnetic characteristics of the TM-$MoSe_2$ system and may also facilitate the implementation of SGS/HM behavior and realization of spintronic devices based on other 2D materials.

Keywords: transition metal dichalcogenides, spin gapless semiconductor, half-metals, strain engineering

Introduction

To improve the performance of spintronic devices, materials with high spin polarization are highly desired [1-3]. Spin gapless semiconductor (SGS), first proposed by Wang [4], not only have the complete spin polarization for electrons and holes, but also have no gap in the electronic spectrum, that is no energy is required to excite

electrons from the valence band to the conduction band. Half-metals (HM), which are metallic in one spin channel and semiconducting in the other spin channel, can achieve complete spin polarization at the Fermi level [5-7]. Due to 100% spin-polarization of the carriers at the Fermi level, SGS and HM materials have been considered as the most promising candidates for applications in spintronics. Therefore, great effort has been focused on searching for SGS and HM materials. Previous studies demonstrated that SGS and HM have been found in a large number of systems, including transition-metal oxides, transition-metal chalcogenides, perovskites, and Heusler compounds [8-10].

Interestingly, SGS and HM behaviors have also been predicted in two-dimensional (2D) materials, such as graphene, transition metal carbides and nitrides (also known as MXenes), and black phosphorus by introducing impurities [11-13], creating defects, [14, 15], and applying strain [16, 17]. Our previous works indicated that gold-embedded zigzag graphene nanoribbons (ZGNRs) can be used as SGS [18], and Pt-embedded ZGNRs exhibit a semiconductor−metal−HM transition as the position of Pt substitutional impurities in the ribbon changes from the center to edge sites [19]. Yafei Li et al. reported the SGS−metal−HF transition in N-doped ZGNRs [11]. The HM behavior was also found when Re atom dopants were at the center of armchair $MoSe_2$ nanoribbon [20]. Fe doped $MoSe_2$ and Mn, Fe, Co, Ni doped WS_2 were reported to exhibit the half-metallic character [21, 22]. In addition to introducing impurities, strain engineering is also an effective approach to tune electronic and magnetic properties of 2D materials [23-25]. For instance, strain generated by wrinkles can induce magnetism and modulate the optical band gap of $ReSe_2$ [26]. It was predicted that band gap of

zigzag BN nanoribbons can be obviously decreased as tensile strain increases [27]. The deformation in monolayer black phosphorus can significantly tune the band gap and induce a transition from semiconductor to metal [28]. Likewise, a direct-to-indirect band gap and a semiconductor-to-metal transition can be caused by mechanical strain in TMDs [29]. Under a biaxial strain, HM and SGS can be observed in monolayer MXenes [16]. The tensile strain can significantly enhance the magnetic moments and gives rise to a half-metallic character in NbS_2 and $NbSe_2$ [30]. By applying strain, the half-fluorinated BN and GaN sheets exhibit intriguing magnetic transitions from ferromagnetism to antiferromagnetism, and a half-metallic behavior can be achieved in the layers under a compressive strain of 6% [31]. In Al-doped $MoSe_2$ monolayer, magnetism was reported to disappear under compressive strain, while the magnetism is preserved under tensile strain [32]. The Co-doped WSe_2 monolayer can transform from magnetic semiconductor to half-metallic material under strain, as the first-principles calculation indicate [33]. The above results indicate that the electronic and magnetic properties of 2D materials are sensitive to the presence of dopants and external strain, so that it is meaningful to search for SGS and HM behavior in such systems.

Transition metal dichalcogenides (TMDs), a class of inorganic 2D materials, have attracted much attention in recent years due to their intriguing electronic, optical and chemical properties [34-36]. $MoSe_2$ monolayer, one of the most studied members of the TMD family, has been successfully fabricated by mechanical exfoliation, chemical vapor deposition (CVD) and molecular beam epitaxy (MBE) [37-41]. Benefiting from the direct band gap of 1.44eV [42, 43] and high carrier mobility [44], $MoSe_2$ monolayer

shows good potentials for applications in various electronic devices including field effect transistors (FET) [45, 46], photodetectors [47] and phototransistors [48].

However, there are few reports on SGS or HM in $MoSe_2$ monolayer to date. In this work, by means of systematic density functional theory (DFT) calculations, we explore the electronic and magnetic properties of MoSe2 with transition metal (TM) atoms (Fe, Co, Ni) embedded into the atomic network in substitutional positions (TM-$MoSe_2$). The results reveal that Fe/Ni-$MoSe_2$ system shows the HM, while Co-$MoSe_2$ exhibits the SGS behavior. Moreover, the SGS/HM is robust in TM-$MoSe_2$ independent of the magnitude of biaxial strain. In contrast, the biaxial strain can effectively modulate the magnetic properties of TM-$MoSe_2$ by controlling the spin polarization of TM-3*d* orbitals. These results suggest that doping and strain engineering is an effective route to achieve SGS/HM behavior and tune the magnetic properties in TM-$MoSe_2$.

Computational methods

Our calculations were carried out using the Vienna ab initio simulation package (VASP) [49, 50] based on DFT. The generalized gradient approximation (GGA) with the Perdew-Burke-Ernzerhof (PBE) [51] parametrization was employed to deal with the exchange-correlation functional. We also tested on-site Coulomb interaction using PBE + U functional [52] to confirm our results. The values of Hubbard term U are 3.5, 2.8 and 3.4 eV for Fe, Co and Ni atoms, respectively [53]. The projector-augmented-wave (PAW) method was used to describe electron-ion interactions [54]. The energy cutoff of the plane wave basis was set to 500 eV. The convergence criterion of the total energy and force were 10^{-6} eV/atom and 0.01 eV/Å, respectively. A k-point sampling

of 11 × 11 × 1 was used for geometry optimizations and self-consistent calculations, and a vacuum region of 15 Å was introduced to avoid interaction between periodic images of the slabs.

Results and discussion

Prior to modelling the substitution of host atoms with Fe, Co, Ni atoms in $MoSe_2$ monolayer, we first checked the accuracy of our approach by evaluating the lattice constant of pristine $MoSe_2$. We found that the optimized lattice constant of $MoSe_2$ monolayer is 3.32 Å, in good agreement with the experimental data [38] and previous theoretical reports [55, 56]. The PBE+U functional also gives the same lattice constant (see Table S1). Doping can be modelled in a 4 × 4 $MoSe_2$ supercell by substituting a Mo or Se atom for Fe, Co, Ni atoms, respectively. The atomic models illustrating the substitutional dopants in the Mo and Se sites in $MoSe_2$ monolayer are shown in Fig. 1. When Fe, Co, Ni (TM) atoms are embedded into the Mo site of $MoSe_2$, the atoms form six covalent bonds with the nearest Se atoms. The bond lengths of TM-Se are 2.41 Å, smaller than that of Mo-Se (2.54 Å). When TM atoms are embedded at the Se site, three covalent bonds are formed between the TM atom and the nearest Mo atom. TM-Mo bond lengths are 2.39 Å, 2.44 Å and 2.51 Å, respectively.

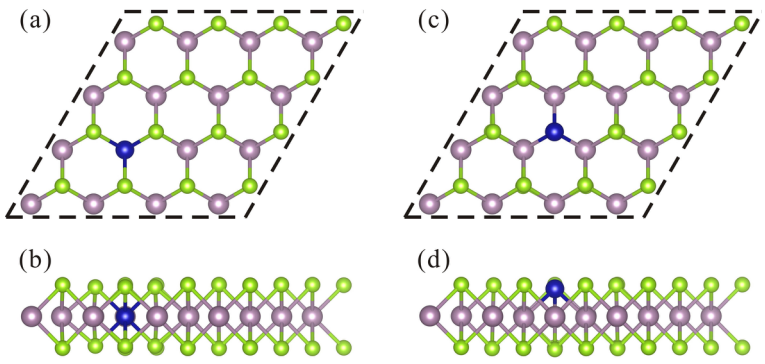

Fig. 1. The top and side views of TM impurity atoms at the Mo or Se sites in the $MoSe_2$ monolayer. The purple and green balls represent Mo and Se atoms, and the blue balls represent the TM atoms (Fe, Co and Ni), respectively.

To assess the energetics and stability of the system with Fe, Co and Ni atoms embedded in $MoSe_2$, we calculated the formation energy of Fe, Co and Ni atoms at different sites of $MoSe_2$ monolayer. The formation energy E_f is defined as $E_f = E_{TM@Mo/Se} + \mu_{Mo/Se} - \mu_{TM} - E_{MoSe_2}$, where $E_{TM@Mo/Se}$ and E_{MoSe_2} are the total energy of TM-$MoSe_2$ and pristine $MoSe_2$ respectively, and μ_{TM} is the chemical potential of TM atom in the isolated TM dimer ($\mu_{TM} = \frac{1}{2}/E_{TM_2}$). We chose dimer as the reference system to assess the stability of the substitutional configurations with regard to clustering on the surface, with the dimer being the smallest cluster. $\mu_{Mo/Se}$ is the chemical potential of Mo/Se atom, which depends on the experimental situation. Here, we assume that μ_{Mo} and μ_{Se} are in a thermal equilibrium with $MoSe_2$, so that $\mu_{Mo} + 2\mu_{Se} = E_{MoSe_2}$[57, 58]. For the Mo-rich condition, μ_{Mo} is calculated from the bulk Mo structure ($\mu_{Mo}^{Mo-rich} = \mu_{Mo,bulk}$), μ_{Se} is taken as $\mu_{Se}^{Mo-rich} = \frac{1}{2}/(E_{MoSe_2} - \mu_{Mo,bulk})$ and defined as 0 eV. Analogously, for the Se-rich condition, μ_{Se} is determined from the Se_2 dimer ($\mu_{Se}^{Se-rich} = \frac{1}{2}/E_{Se_2}$), μ_{Mo} is calculated as $\mu_{Mo}^{Se-rich} = E_{MoSe_2} - 2\mu_{Se,Se_2}$. According to the above definition, a more negative E_f value indicates a higher stability of the TM-$MoSe_2$. The calculated values of formation energy are presented in Fig. 2. It is evident that the TM@Mo configurations are energetically more favorable under the Se-rich condition, which is consistent with the recent reports [21, 59]. E_f values exhibit a following trend: $E_{f(Fe)}$ (-4.34 eV) < $E_{f(Co)}$

(-3.67 eV) < $E_{f(Ni)}$ (-2.51 eV) in the Se-rich limit, indicating that the Fe@Mo system is more energetically favorable than the others. We performed test calculations of the formation energy using the PBE+U functional, and found that the trend of $E_{f(Fe)}$ (-3.35 eV) < $E_{f(Co)}$ (-3.22 eV) < $E_{f(Ni)}$ (-2.39 eV) is the same in the Se-rich limit (see Table S1). Different from the TM@Mo case, the TM@Se configurations are more favorable under the Mo-rich condition. However, as TM impurities at the Mo positions are energetically more favorable in a wider range of Se chemical potential, we focus on the electronic and magnetic properties of $MoSe_2$ monolayer with the former.

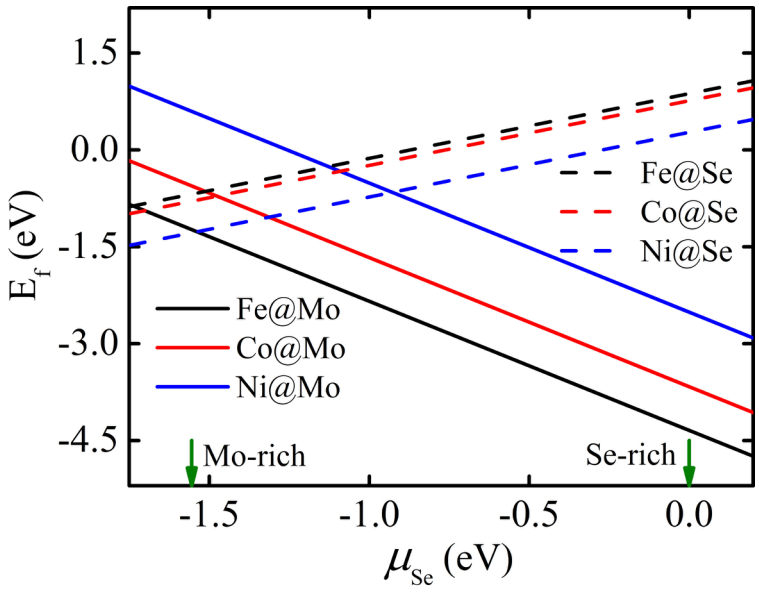

Fig. 2. Formation energies of TM impurities at Mo/Se sites in MoSe2 sheet as functions of Se atom chemical potential μ_{Se}.

In order to get insight into the magnetic properties of TM-$MoSe_2$, the spin-densities in these systems are shown in Fig. 3. It can be seen that the spin densities are mainly localized on TM atoms and the neighboring Mo atoms. The local magnetic moments of TM atoms exhibit a trend of M_{Ni} (0.25 μ_B) < M_{Co} (0.88 μ_B) < M_{Fe} (1.38 μ_B). The neighboring Mo atoms have the magnetic moments of 0.11, 0.22 and 0.19 μ_B in

Fe-, Co- and Ni-$MoSe_2$, respectively. For Fe-$MoSe_2$, the total magnetic moment is 2.00 μ_B, mostly coming from the Fe atom and partly from its neighboring Mo atoms. The total magnetic moments of Co-$MoSe_2$ and Ni-$MoSe_2$ are 2.67 and 1.89 μ_B, which mainly stem from the neighboring Mo atoms and partly from Co/Ni atoms. The PBE+U calculations were also performed. The total magnetic moments of Fe-$MoSe_2$, Co-$MoSe_2$ and Ni-$MoSe_2$ are 2.00, 2.75, 1.86 μ_B with PBE+U method, respectively. There are no noticeable changes for magnetic moments of TM-$MoSe_2$ (see Table S1), confirming our results.

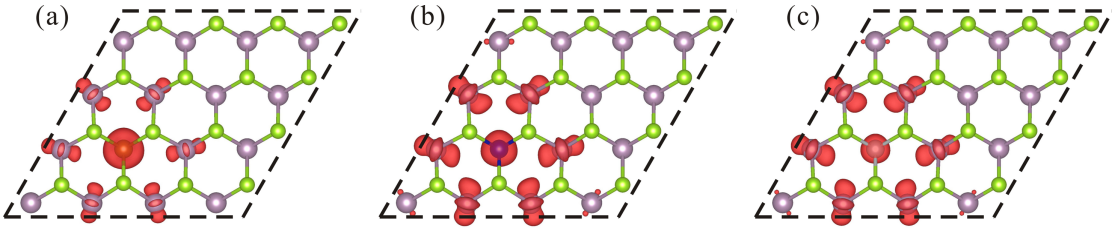

Fig. 3. Spin-density distribution of (a) Fe-, (b) Co- and (c) Ni-$MoSe_2$. The isosurface is set to be 0.004 e/Å^3. The red regions represent spin-up density.

To investigate the effects of TM impurities on the electronic properties of $MoSe_2$ monolayer, the spin-polarized band structures were calculated and presented in Fig. 4. At the PBE level of theory, the pristine $MoSe_2$ exhibits a direct band gap of 1.44 eV, which agrees well with previously reported values [55, 56]. After TM atom introduction, flat impurity states can be clearly observed in the band gap of $MoSe_2$. For Fe-$MoSe_2$, it is evident from Fig. 4(a) that the spin-up channel is metallic with a band crossing the Fermi level, while the spin-down channel remains semiconducting with a gap of 0.91 eV. Therefore, Fe-$MoSe_2$ presents HM character and can provide 100% spin-polarized current. Co-$MoSe_2$ exhibits a semiconducting character with a band gap of 0.42 and

0.75 eV for the spin-up and spin-down channels, respectively, as indicated in Fig. 4(b). Interestingly, the valence band maximum (VBM) of the spin-up channel and the conduction band minimum (CBM) of the spin-down channel are both at the K point, and the band gap is 0.06 eV. According to Wang and Hu [4, 18], the band gap of approximately 0.1 eV or less than 0.1 eV can be defined as “gapless”. Thus, the band structure can be assumed to be gapless, which means that Co-$MoSe_2$ shows an SGS behavior. As for Ni-$MoSe_2$, the spin-up channel is semiconducting with a gap of 0.21 eV, while the spin-down VBM crosses the Fermi level and displays metallicity (see Fig. 4(c)). Thus, Ni-$MoSe_2$ is also HM, similar to the case of Fe-$MoSe_2$. The corresponding charge densities of the bands near the Fermi level (indicated by the red and blue dashed lines) are presented in the right panel of Fig. 4, which indicates that the spin-up and spin-down states near the Fermi level mainly come from TM atoms and the neighboring Mo atoms in all cases.

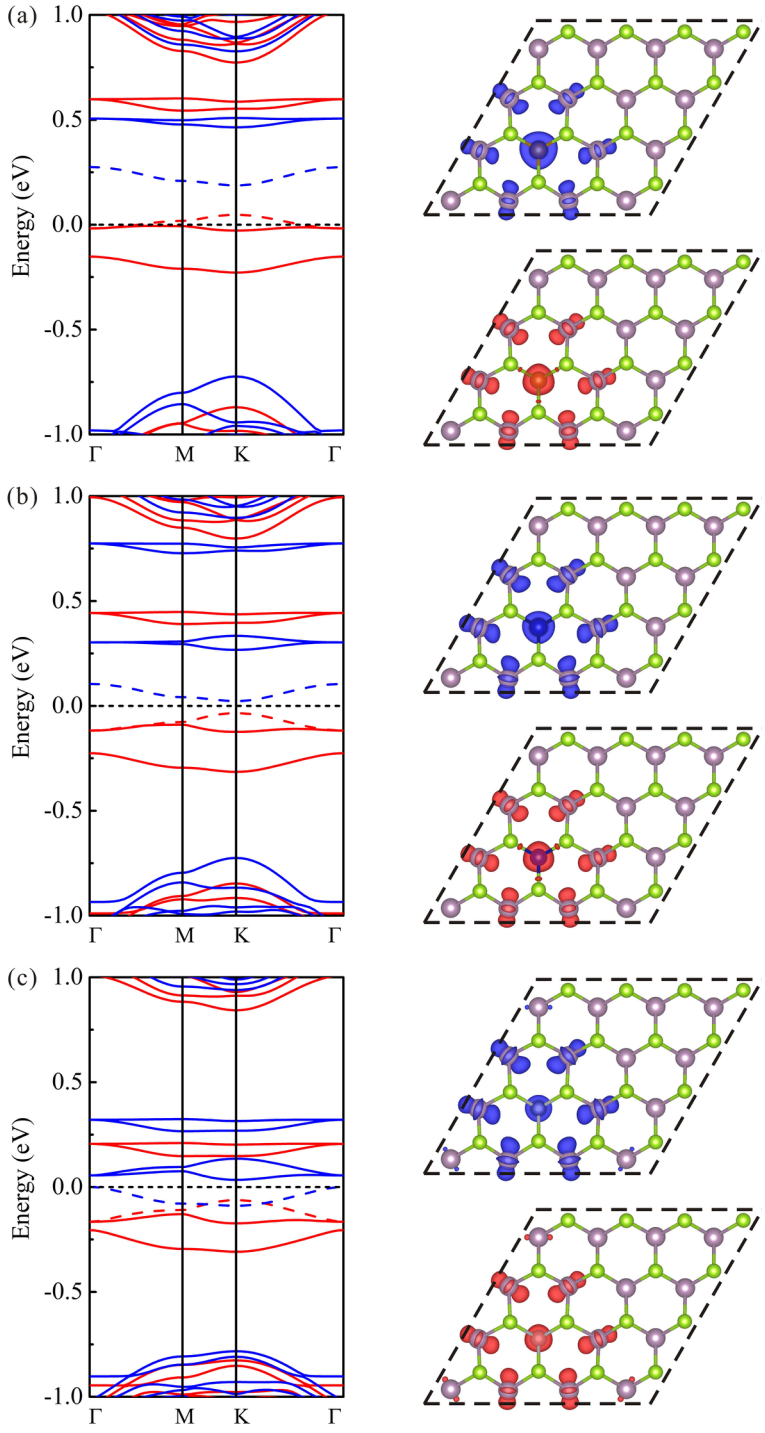

Fig. 4. Band structures and the corresponding charge densities of the bands (indicated by the red and blue dashed lines) near the Fermi level for (a) Fe-, (b) Co- and (c) Ni-$MoSe_2$. The red and blue solid lines indicate spin-up and spin-down channels in the band structures, respectively. The positions of the Fermi level is indicated by the black dashed lines. The red and blue regions refer to the spin-up and spin-down states, respectively. The isosurface is set to be 0.004 e/Å^3.

Next, to gain a deeper understanding of the changes in the electronic structure for TM-$MoSe_2$, we also calculated the projected density of states (PDOS), which are presented in Fig. 5. In the pristine $MoSe_2$ monolayer, the CBM is mainly dominated by the Mo d_{z^2} orbitals, while the VBM is mostly described by the Mo d_{xy}+d_{x^2} orbitals (Fig. 5(a)), consistent with the previously obtained results [55, 56]. Upon embedding TM atoms, it is clear from Fig.5 that the bands near the Fermi level are spin polarized. Specifically, for Fe-$MoSe_2$, two PDOS peaks were observed near the Fermi level for the spin-up channel, which are dominated by the Fe d_{xy}+d_{x^2} and Mo d_{z^2} orbitals, as illustrated in Fig. 5(b), while the spin-down channel remains semiconducting. Thus, Fe-$MoSe_2$ is HM with 100% spin-polarized current near the Fermi level. For Co-$MoSe_2$, Co atom induces impurity states in the energy range of -0.5 to 0.5 eV. The spin-up impurity states near the Fermi level are mainly composed of the Co d_{xy}+d_{x^2} and Mo d_{z^2} orbitals, while the spin-down impurity states near the Fermi level are dominated by the d_{z^2} orbitals of Co and Mo atoms. In Ni-$MoSe_2$, the spin-up channel is still semiconducting, whereas the spin-down channel is gapless, with the states mainly contributed by the Ni d_{xy}+d_{x^2}, d_{z^2} and Mo d_{z^2} orbitals. Therefore, Ni-$MoSe_2$ shows half-metallicity, similar to the case of Fe-$MoSe_2$. These results indicate that SGS and HM can be obtained in the $MoSe_2$ monolayer by introducing Fe, Co and Ni atoms.

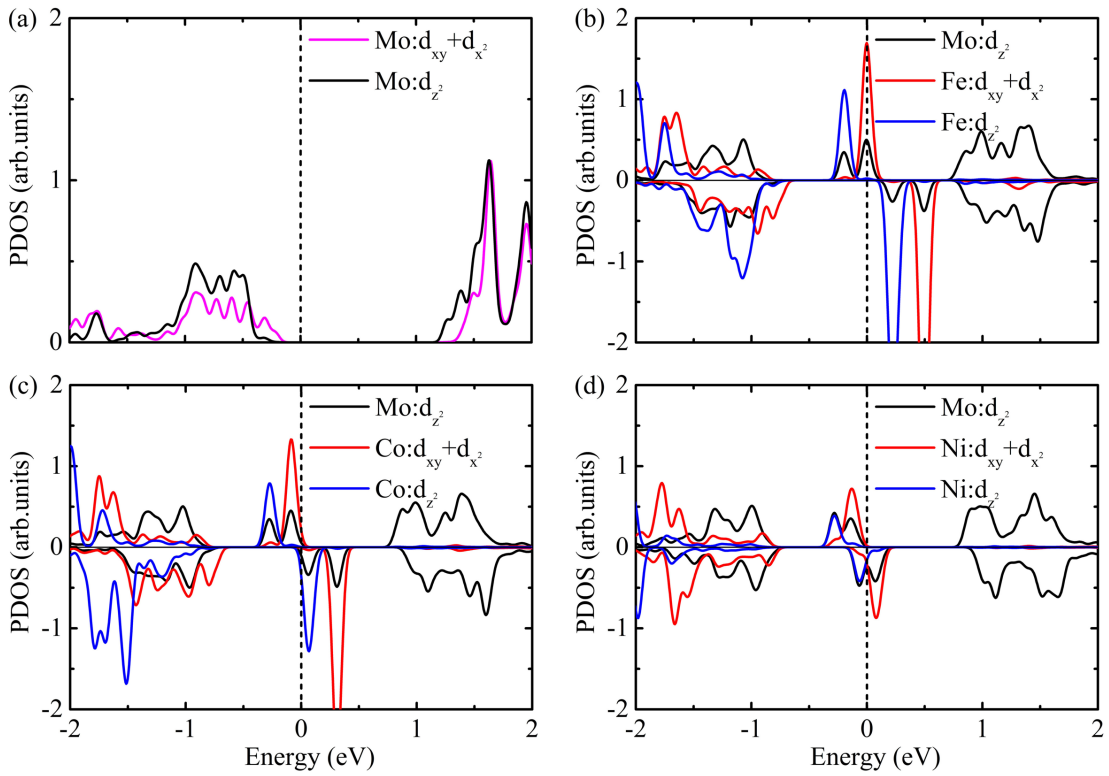

Fig. 5. (a) PDOS of pristine $MoSe_2$. PDOS of (b) Fe-, (b) Co- and (c) Ni-$MoSe_2$. The black dashed lines indicate the positions of the Fermi level. The positive and negative values represent spin-up and spin-down channels, respectively.

Previous studies suggested that the external strain can play an important role in practical applications of 2D materials, as it can effectively tune the electronic and magnetic properties of various 2D systems, such as graphene, MoS_2, BN and GaN [27-31]. We also studied the effects of strain on TM-embedded $MoSe_2$. The biaxial strain was defined as $\varepsilon = \Delta c/c_0$, where the unstrained and strained lattice constants of TM-$MoSe_2$ are c_0 and $c = c_0 \pm \Delta c$, respectively. The tensile or compression strain was modeled by first increasing lattice constant c, then reoptimizing the atomic structure with the elongated lattice constant kept fixed. We investigated the strain dependence of the magnetic moment in TM-$MoSe_2$ by varying the strain from -5% to 5%, as shown in Fig. 6. It can be seen that the variation of magnetic moments with strain is drastically

different for the Fe-$MoSe_2$, Co-$MoSe_2$ and Ni-$MoSe_2$ systems. For the Fe-$MoSe_2$, the magnetic moment is 2 μ_B for strain values from -4% to 5%, which is due to the spin polarization of the Fe 3*d* orbital near the Fermi level, which does not changed. However, at a compressive strain of 5%, spin polarization of the Fe 3*d* orbital decreases, as evident from the shifts of the α and β states in PDOS (Fig. 7(a)), leading to a significant reduction of magnetic moment by 26.5% as compared to the unstrained Fe-$MoSe_2$. The magnetic moment of Co-$MoSe_2$ increases monotonously with increasing biaxial strain from -5% to 5%. The reason for such a behavior is that the spin polarization of the Co 3*d* orbital around the Fermi level increases with increasing strain (Fig. 7(b)). As for Ni-$MoSe_2$, the magnetic moment does not noticeably change under tensile strain. In contrast, the magnetic moment of Ni-$MoSe_2$ initially increases to a maximum of 2.37 μ_B at -2% strain, and then decreases with further increasing compressive strain (Fig. 6). It can be concluded that the biaxial strain can effectively modulate the magnetic properties of TM-$MoSe_2$ by controlling spin polarization of the 3*d* orbitals of TM atoms.

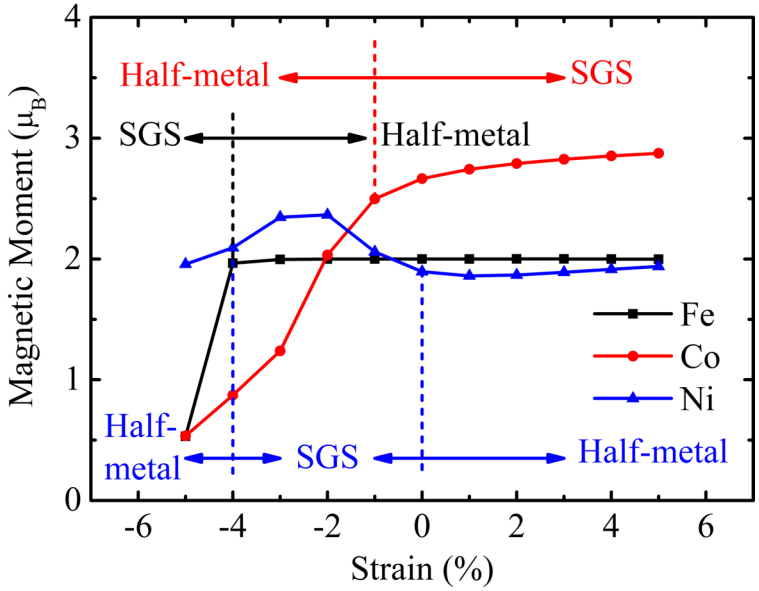

Fig. 6. Magnetic moments and electronic characteristics of Fe-, Co- and Ni-$MoSe_2$ under biaxial

strain.

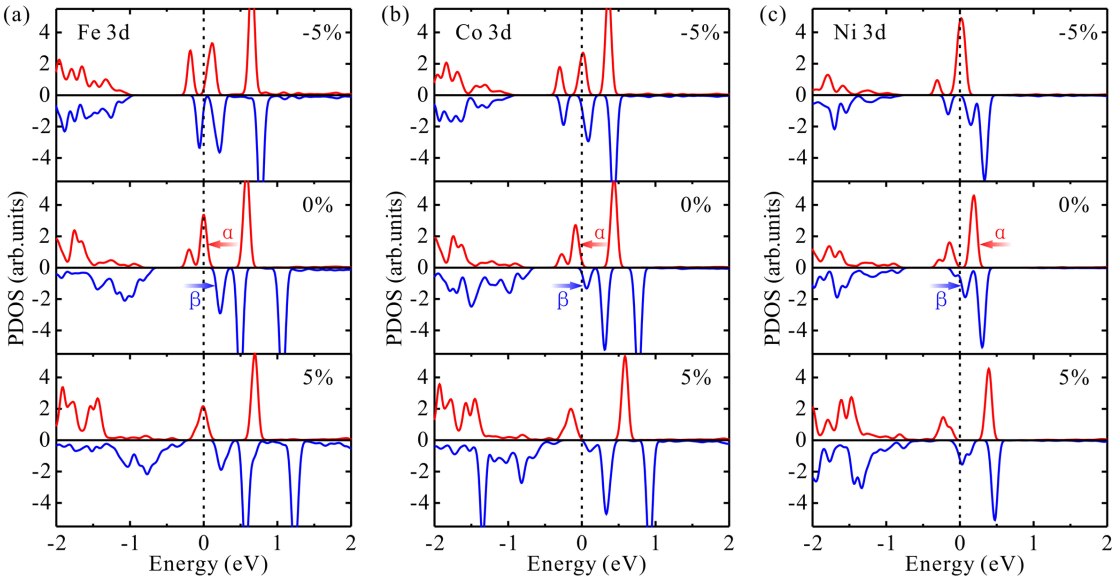

Fig. 7. PDOS of (a) Fe-, (b) Co- and (c) Ni-$MoSe_2$ under -5%, 0% and 5% biaxial strain, respectively. The red and blue solid lines indicate spin-up and spin-down channels, respectively. The Fermi level position is indicated by the black dashed lines.

Further, we analyzed the electronic properties of TM-$MoSe_2$ under biaxial strain. The electronic characteristics and band structures are displayed in Fig. 6 and Fig. 8. It is found that the HM can be preserved in Fe-$MoSe_2$ in a strain range from -4% to 5%, while an interesting transition from HM to SGS takes place at a compressive strain of -5%. The Co-$MoSe_2$ preserves its SGS behavior in a strain range from -1% to 5%, and becomes HM under compressive strain larger than 1%. As for Ni-$MoSe_2$, HM characteristics persist at tensile strain and a compressive strain of -5%, while it shows SGS behavior in the range of compressive strain from 0% to -4%. Our results suggest that TM-$MoSe_2$ remains the robust SGS/HM system regardless of the biaxial strain value. We studied the electronic properties of TM-$MoSe_2$ under strain using the PBE + U functional, as shown in Table S2. It is found that TM-$MoSe_2$ also preserves the HM

or SGS properties.

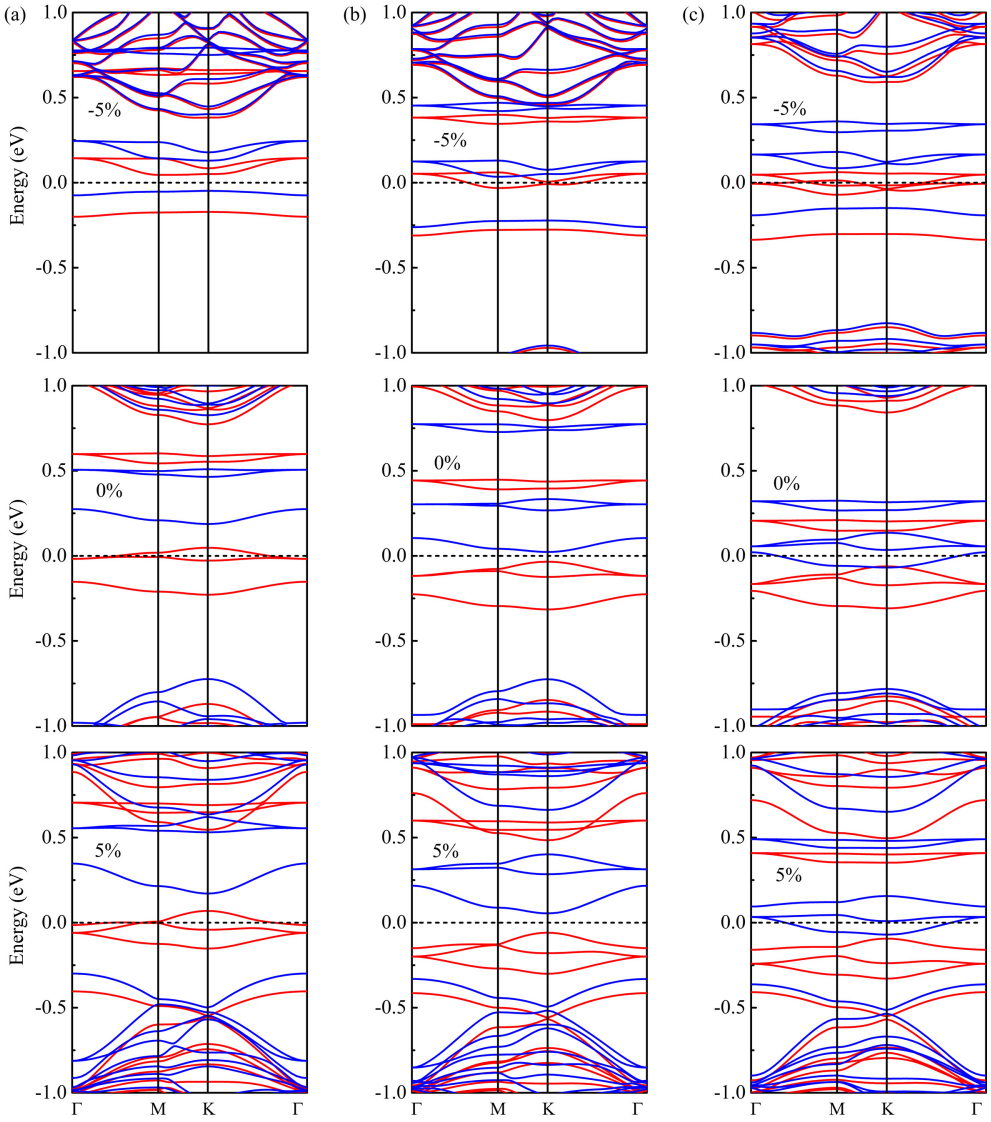

Fig. 8. Band structures of (a) Fe-, (b) Co- and (c) Ni-$MoSe_2$ under -5%, 0% and 5% biaxial strain, respectively. The red and blue solid lines indicate spin-up and spin-down channels in the band structures, respectively. The Fermi level position is indicated by the black dashed lines.

Conclusions

In summary, we have systematically investigated the electronic and magnetic properties of TM-$MoSe_2$ by means of DFT calculations. It is demonstrated that $MoSe_2$ sheet with Fe/Ni impurities shows the HM character, whereas Co-$MoSe_2$ exhibits an SGS behavior. Interestingly, the SGS/HM of TM-$MoSe_2$ can be well preserved

regardless of biaxial strain value. In addition, Fe, Co, Ni atom substitutional impurities can induce magnetism in $MoSe_2$ monolayer. The magnetic moments of TM-$MoSe_2$ can be effectively tuned under the biaxial strain by controlling spin polarization of the 3*d* orbitals of Fe, Co, Ni atoms. Experimentally, strain engineering of 2D materials can be achieved by lattice constant mismatch, thermal-expansion mismatch, or transferring them on a flexible substrate and directly stretching, compressing, or bending the substrate [60]. Our results offer a new route to designing the SGS/HM properties and modulating magnetic characteristics of TM-$MoSe_2$ system and may also facilitate the implementation of SGS/HM behavior and realization of spintronic devices based on other 2D materials.

Acknowledgements

This work is supported in China by the National Natural Science Foundation of China (Nos.11604047, 51672127), the Natural Science Foundation of Jiangsu Province (No. BK20160694), Jiangsu Planned Projects for Postdoctoral Research Funds (No. 2019K010A), the Priority Academic Program Development of Jiangsu Higher Education Institutions (PAPD), the Fundamental Research Funds for the Central Universities, and the open research fund of Key Laboratory of MEMS of Ministry of Education, Southeast University. AVK acknowledges funding from the German Research Foundation (DFG), project KR 48661/2 We also thank the High Performance Computing Center of Nanjing Tech University and CSC Finland for generous grants of computer time.

References

[1] Žutić I, Fabian J and Sarma S D 2004 *Rev. Mod. Phys.* **76** 323

[2] Felser C, Fecher G H and Balke B 2007 *Angew. Chem. Int. Ed.* **46** 668-99

[3] Liu W and Xu Y 2016 *Curr. Opin. Solid State Mater. Sci.* **20** 388-95

[4] Wang X L 2008 *Phys. Rev. Lett.* **100** 156404

[5] De Groot R A, Mueller F M, Van Engen P G and Buschow K H J 1983 *Phys. Rev. Lett.* **50** 2024

[6] Wang X L, Dou S X and Zhang C 2010 *NPG Asia Mater.* **2** 31-8

[7] Li X and Yang J 2017 *WIREs Comput. Mol. Sci.* **7** e1314

[8] Li X and Yang J 2016 *Natl. Sci. Rev.* **3** 365-81

[9] Graf T, Felser C and Parkin S S P 2011 *Prog. Solid State Chem.* **39** 1-50

[10] Ouardi S, Fecher G H, Felser C, and Kübler J 2013 *Phys. Rev. Lett.* **110** 100401

[11] Li Y, Zhou Z, Shen P, and Chen Z 2009 *ACS Nano* **3** 1952-8

[12] Wang Y, Song N, Dong N, Zheng Y, Yang X, Jiang W, Xu B and Wang J 2019 *Appl. Surf. Sci.* **480** 802-9

[13] Xu R, Liu B, Zou X and Cheng H M 2017 *ACS Appl. Mater. Interfaces* **9** 38796-801

[14] Du A, Chen Y, Zhu Z, Amal R, Lu G Q and Smith S C 2009 *J. Am. Chem. Soc.* **131** 17354-9

[15] Guan J, Yu G, Ding X, Chen W, Shi Z, Huang X and Sun C 2013 *ChemPhysChem* **14** 2841-52

[16] Gao G, Ding G, Li J, Yao K, Wu M and Qian M 2016 *Nanoscale* **8** 8986-94

[17] Wu Z, Yu J and Yuan S 2019 *Phys. Chem. Chem. Phys.* **21** 7750-5

[18] Hu X, Zhang W, Sun L and Krasheninnikov A V 2012 *Phys. Rev. B* **86** 195418

[19] Hu X, Wan N, Sun L and Krasheninnikov A V 2014 *J. Phys. Chem. C* **118** 16133-9

[20] Zhao X, Zhang H, Sun M, Wang T, Wei S and Dai X 2020 *Physica E* **118** 113872

[21] Tian Y, Zhu Z, Ge Z, Sun A, Zhang Q, Huang S, Li H and Meng J 2020 *Physica E* **116** 113745

[22] Xie L Y and Zhang J M 2016 *Superlattices Microstruct.* **98** 148-57

[23] Ma Y, Dai Y, Guo M, Niu C, Zhu Y and Huang B 2012 *ACS Nano* **6** 1695-701

[24] Wang Y, Wang S S, Lu Y, Jiang J and Yang S A 2016 *Nano Lett.* **16** 4576-82

[25] Zhang Z, Zhao Y and Ouyang G 2017 *J. Phys. Chem. C* **121** 19296-304

[26] Yang S *et al* 2015 *Nano Lett.* **15** 1660-6

[27] Qi J, Qian X, Qi L, Feng J, Shi D and Li J 2012 *Nano Lett.* **12** 1224-8

[28] Rodin A S, Carvalho A and Neto A H C 2014 *Phys. Rev. Lett*. **112** 176801

[29] Johari P and Shenoy V B 2012 *ACS Nano* **6** 5449-56

[30] Zhou Y, Wang Z, Yang P, Zu X, Yang L, Sun X and Gao F 2012 *ACS Nano* **6** 9727-36

[31] Ma Y, Dai Y, Guo M, Niu C, Yu L and Huang B 2011 *Nanoscale* **3** 2301-6

[32] Luo M and Shen Y H 2019 *J. Supercond. Novel Magn.* **32** 1105-14

[33] Wu N, Zhao X and Wang T 2016 *Physica E* **84** 505-10

[34] Wang Q H, Kalantar-Zadeh K, Kis A, Coleman J N and Strano M S 2012 *Nat. Nanotechnol.* **7** 699-712

[35] Chhowalla M, Shin H S, Eda G, Li L J, Loh K P and Zhang H 2013 *Nat. Chem.* **5**

263-75

[36] Liu G B, Xiao D, Yao Y, Xu X and Yao W 2015 *Chem. Soc. Rev.* **44** 2643-63

[37] Ceballos F, Bellus M Z, Chiu H Y and Zhao H 2014 *ACS Nano* **8** 12717-24

[38] Chang Y H *et al* 2014 *ACS Nano* **8** 8582-90

[39] Chen T, Hao G, Wang G, Li B, Kou L, Yang H, Zheng X and Zhong J 2019 *2D Mater.* **6**

[40] Xenogiannopoulou E *et al* 2015 *Nanoscale* **7** 7896-905

[41] Poh S M *et al* 2018 *ACS Nano* **12** 7562-70

[42] Zhang Y *et al* 2014 *Nat. Nanotechnol.* **9** 111-5

[43] Hu X, Kou L and Sun L 2016 *Sci. Rep.* **6** 31122

[44] Rhyee J S *et al* 2016 *Adv. Mater.* **28** 2316-21

[45] Chuang H J, Chamlagain B, Koehler M, Perera M M, Yan J, Mandrus D, Tománek D and Zhou Z 2016 *Nano Lett.* **16** 1896-902

[46] Liao W, Wei W, Tong Y, Chim W K and Zhu C 2017 *Appl. Phys. Lett.* **111** 082105

[47] Jung C *et al* 2015 *Sci. Rep.* **5** 15313

[48] Lee H, Ahn J, Im S, Kim J and Choi W 2018 *Sci. Rep.* **8** 11545

[49] Kresse G and Furthmüller J 1996 *Phys. Rev. B* **54** 11169-86

[50] Kresse G and Furthmüller J 1996 *Comput. Mater. Sci.* **6** 15-50

[51] Perdew J P, Burke K and Ernzerhof M 1996 *Phys. Rev. Lett.* **77** 3865-8

[52] Dudarev S L, Botton G A, Savrasov S Y, Humphreys C J and Sutton A P 1998 *Phys. Rev. B* **57** 1505-9

[53] Raebiger H, Lany S and Zunger A 2009 *Phys. Rev. B* **79** 165202

[54] Blochl P E 1994 *Phys. Rev. B* **50** 17953-79

[55] Hu X, Wang Y, Shen X, Krasheninnikov A V, Sun L and Chen Z 2018 *2D Mater.* **5** 031012

[56] Ai W, Kou L, Hu X, Wang Y, Krasheninnikov A V, Sun L and Shen X 2019 *J. Phys. Condens. Matter* **31** 445301

[57] Komsa H P and Krasheninnikov A V 2015 *Phys. Rev. B* **91** 125304

[58] Karthikeyan J, Komsa H P, Batzill M and Krasheninnikov A V 2019 *Nano Lett.* **19** 4581-7

[59] Zhao Y, Tu J, Sun Y, Hu X, Ning J, Wang W, Wang F, Xu Y and He L 2018 *J. Phys. Chem. C* **122** 26570-5

[60] Dai Z, Liu L, Zhang Z 2019 *Adv. Mater.* **31** 1805417